New Models for Predicting Pedestal Temperature and Density in ELMy *H*-Mode Plasma

W. Buangam[1], T. Onjun[2], S. Suwanna[2], and W. Singhsomroje[1]
[1]Department of Physics, Faculty of Science, Mahidol University, Bangkok, Thailand
[2] School of Manufacturing Systems and Mechanical Engineering, Sirindhorn International Institute of Technology, Thammasat University, Khlong Lhuang, Pathum Thani, Thailand

Abstract

Theoretical based models for predicting the temperature and density at the top of the pedestal for types I, II and III ELMy *H*-mode plasmas are developed by using an estimation of plasma thermal energy within the pedestal region and the plasma energy confinement time. Predictions from these pedestal models are compared with experimental data from the ITPA Pedestal Database version 3.2. Statistical analyses, including root-mean square errors (RMSE) and offset values, are performed to quantify the predictive capability of the models. It is found that the theoretical based model for predicting the pedestal electron temperature values in types I, II and III ELMy *H*-mode plasmas yields an RMSE of 27-30%, 8-15% and 31-37%, respectively. The predicted pedestal ion temperature values in types I, II and III ELMy *H*-mode plasmas have RMSE values of 37-72%, 10-11% and 23-24%, respectively. The theoretical based model for predicting the pedestal density values in types I, II and III ELMy *H*-mode plasmas yields an RMSE of 27-30%, 8-16% and 22-30%, respectively.

Keywords: Pedestal, ELMy *H*-mode plasma

1. Introduction

High confinement mode (H-mode) discharges in a tokamak are characterized by a narrow region of plasma profile which has steep pressure gradient at the edge of the plasma, called the pedestal. It acts as a barrier to confine the energy and particles to a plasma core. This leads to increased fusion performance. H-mode discharges are often perturbed by quasi-periodic bursts of energy and particles in the region near the edge of the plasma called Edge Localized Modes or (ELMs). However, ELMs can also be beneficial to impurity removal at the plasma edge region [1].

At the top of the pedestal region, values of pedestal parameter such as temperature, pedestal pressure, and pedestal density are used as boundary conditions connecting the core region and the pedestal region. These boundary conditions allow one to simulate plasma profiles from the pedestal inward to the center [2, 3]. Due to this reason, it is very important to develop accurate temperature and density models at the top of the pedestal region.

In previous studies of pedestal models, it is assumed that thermal conduction losses are the dominant loss mechanisms in the pedestal and that thermal losses are associated with ELM. The scaling of energy loss mechanism from the pedestal can be found in Refs [4-6]. In particular, Ref [6] predicted a pedestal temperature

based on thermal conduction for type I ELMy H-mode discharges.

In this study, the pedestal temperature and density models are developed for types I, II, and III ELMy *H*-mode plasmas. These models are developed based on an estimation of plasma thermal energy within the pedestal region and the plasma energy confinement time.

The predicted results are compared with experimental results from the ITPA Pedestal Database (Version 3.2) [3]. Following [2], statistical analyses such as root-mean-square errors (RMSE) and offset values are calculated to quantify the agreement.

This article is organized into four parts. Pedestal temperature and density models based on energy distribution with *H*-mode scaling laws are described in Section 2. The results and discussions from our statistical analysis are included in Section 3. Finally, conclusions are summarized in Section 4.

2. Pedestal temperature model

In a tokamak plasma, there is a continuous loss of energy which has to be replenished by plasma heating. The average energy of plasma particles at a temperature T is $\frac{3}{2}kT$, comprised of $\frac{1}{2}kT$ per degree of freedom, where *k* is Boltzmann's constant. Since there is an equal number of electrons and ions, the total plasma energy per unit volume is $3nkT$. Therefore the total energy in the plasma can be found as:

$$W = \int 3nkTd^3x$$

$$= 3nkTV \qquad (1)$$

The energy loss from the pedestal is mainly due to the thermal conduction down the steep edge gradient characterizing the pedestal region. The thermal energy at the pedestal can be taken as:

$$W_{ped} = 3n_{ped}kT_{ped}V$$

or

$$W_{ped} = c_1 n_{ped}(\frac{T_{e,ped} + T_{i,ped}}{2})kV$$

where c_1 is 3, n_{ped} is the pedestal density, T_{ped} is the pedestal temperature which is composed of pedestal electron temperature or $T_{e,ped}$, and pedestal ion temperature or $T_{i,ped}$, and V is the plasma volume. The thermal energy at the pedestal can be estimated by:

$$W_{ped} = c_1 kVn_{ped}T_{i,ped}(1+\frac{T_{e,ped}}{T_{i,ped}})$$

or $$W_{ped} = c_2 kVn_{ped}T_{i,ped} \qquad (2)$$

when $c_2 = c_1(1+\frac{T_{e,ped}}{T_{i,ped}})$

$$W_{ped} = c_1 kVn_{ped}T_{e,ped}(1+\frac{T_{i,ped}}{T_{e,ped}})$$

$$W_{ped} = c_3 kVn_{ped}T_{e,ped} \qquad (3)$$

when $c_3 = c_1(1+\frac{T_{i,ped}}{T_{e,ped}})$

and the plasma volume can be estimated by:

$$V = 2\pi^2 Ra^2\kappa\left(1-\frac{\delta a}{4R}-\frac{\delta^2}{4}\right) \qquad (4)$$

where κ and δ are the elongation and triangularity at the separatrix, respectively; *R* and *a* are major radius and minor radius of a tokamak.

Moreover, W_{ped} can also be computed from the total thermal energy W_{th} in the system, namel:

$$W_{ped} = c_4 W_{th} \tag{5}$$

where c_4 is a fraction of total thermal energy at the pedestal and is often estimated by taking c_4 = 0.35. This value is standard highly radiative nitrogen seeded ELMy H-Mode with type III ELMs scenario [7]. Here we leave the constants c_2, c_3 , and c_4 undetermined.

In present tokamaks the thermo-nuclear power is usually small and in steady state. The rate of energy loss, P_L, is balanced by externally supplied heating to the plasma, P_{aux}, which is characterized by energy confinement time, τ_E, defined by the relation:

$$P_{aux} = P_L = c_4 \frac{W_{th}}{\tau_E} \tag{6}$$

where P_{aux} is an auxiliary heating power, which generally comes from neutral beam injection (NBI) or radio frequency (RF) heating. Combining Eqs. (2), (3), (5), and (6) the resulting pedestal ion temperature is:

$$T_{e,ped} = C_{E,e} \frac{P_{aux}\tau_E}{n_{ped} kV} \tag{7}$$

the pedestal electron temperature is:

$$T_{i,ped} = C_{E,i} \frac{P_{aux}\tau_E}{n_{ped} kV} \tag{8}$$

and pedestal density is:

$$n_{ped} = C_{E,n} \frac{P_{aux}\tau_E}{T_{ped} kV} \tag{9}$$

where $C_{E,e}$, $C_{E,i}$ and $C_{E,n}$ are the constants to be determined as to minimize the root-mean-square errors (RMSE) of predicted results when they are compared with experimental data. In Eqs. (7)-(9), all relevant quantities, except τ_E, are known from each tokamak; and they describe either an experimental scheme or the geometry of plasma in the tokamak.

2.1 Scaling laws for energy confinement time

The quantity τ_E is deduced in various ways from many experiments. There already exist several scaling laws that can estimate τ_E in terms of plasma engineering parameters [8-10] as published by the ITER Physics Basis (IPB) group [1]. Here, we employ four well-known scaling laws whose expressions of the thermal energy confinement time τ_E of ELMy *H*-mode plasma are included below.

In the following expressions, *I* denotes current in MA, *B* is toroidal field in T, *P* is power in MW, *n* is density in $(\times 10^{19} m^{-3})$, *R* is major radius in *m*, and *M* is effective mass in *amu*. An inverse aspect ratio, ε = *a/R*, and elongation κ are dimensionless.

$$\tau_{ITERH-93P} = 0.036 I^{1.06} B^{0.32} P^{-0.67} n^{0.17} R^{1.79} \varepsilon^{-0.11} \kappa^{0.66} M^{0.41}$$

$$\tau_{ITERH-ESP97(y)} = 0.029 I^{0.90} B^{0.20} P^{-0.66} n^{0.40} R^{2.03} \varepsilon^{0.19} \kappa^{0.92} M^{0.2}$$

$$\tau_{IPB98(y,3)} = 0.0564 I^{0.88} B^{0.07} P^{-0.69} n^{0.40} R^{2.15} \varepsilon^{0.64} \kappa^{0.78} M^{0.2}$$

$$\tau_{IPB98(y,4)} = 0.0587 I^{0.85} B^{0.29} P^{-0.70} n^{0.39} R^{2.08} \varepsilon^{0.69} \kappa^{0.76} M^{0.17}$$

More details and excellent overviews of these scaling laws can be found in [9-13].

3. Results and discussion

The experimental data used in this work are taken from the International Pedestal Database (version 3.2) from five tokamaks: the Axially Symmetric Divertor Experiment (ASDEX-Upgrade or AUG),

the Joint European Torus tokamak (JET), the upgraded Japan Atomic Energy Research Institute Tokamak-60 (JT-60U), Doublet-III D (DIII-D), and the Mega Amp Spherical Tokamak (MAST). The experimental data for pedestal electron temperature, pedestal ion temperature and pedestal density in types I, II, and III ELMy H-mode plasmas are listed in Table 1.

Table 1 Summary of the experimental data for pedestal electron temperature (T_e), pedestal ion temperature (T_i) and pedestal density (n_e) in types I, II, and III ELMy H-mode.

		AUG	JET	JT-60U	DIII-D	MAST	Total
Type I	T_e	125	116	365	97	-	703
	T_i	-	90	388	-	-	478
	n_e	125	116	365	97	-	703
Type II	T_e	3	-	24	-	-	27
	T_i	-	-	24	-	-	24
	n_e	3	-	24	-	-	27
Type III	T_e	132	17	44	67	5	265
	T_i	-	14	43	-	-	57
	n_e	132	17	44	67	5	265

Statistical analysis such as the root mean-square error (RMSE) and the offset value are used to quantify the comparison between the predictions of each model and experimental data. The RMSE of each quantity x (T_e, T_i, n_e) is defined as:

$$RMSE(\%) \equiv \sqrt{\frac{1}{N-1}\sum_{j=1}^{N}(\ln(X_{\exp_j}) - \ln(X_{\mathrm{mod}_j}))^2} \times 100 \quad (10)$$

And the offset, as:

$$Offset \equiv \frac{1}{N}\sum_{j=1}^{N}(\ln(X_{\exp_j}) - \ln(X_{\mathrm{mod}_j})), \quad (11)$$

where N is total number of data points, and $X_{\exp_j}$ and X_{mod_j} are the jth data point of the experiment and the model, respectively.

3.1 Results

Statistical analysis is used to compare between the predictions of each model and experimental data. The RMSE% and offset values from the model based on energy distribution coupled with four scaling laws for types I, II and III ELMy *H*-Mode plasma are shown in Table 2-4, respectively. Table 2 summarizes the RMSE% [Eq. (10)] and offset values [Eq. (11)] from each model in type I ELMy *H*-Mode plasma, compared with the experimental data, for pedestal electron temperature and pedestal density models composed of 703 data points and 478 data points for pedestal ion temperature. It is found that the ITERH-EPS97y scaling law for energy confinement time gives the best agreement with experiments, yielding RMSE of 27.12% for pedestal electron temperature and pedestal density, while ITERH-93P scaling law gives the best agreement with experiments, for pedestal ion temperature yielding RMSE of 37.59%. Table 3 summarizes the RMSE% and offset values from each model in type II ELMy *H*-Mode plasma compared with the experimental data, for pedestal electron temperature and pedestal density models composed of 27 data points and 24 data points for pedestal ion temperature. It is found that the IPB98(y,3) scaling law for energy confinement time gives the lowest RMSE of 8.41% for pedestal electron temperature and pedestal density, while ITERH-EPS97y

scaling law gives the lowest RMSE of 10.96% for pedestal ion temperature. Table 4 summarizes the RMSE% and offset values from each model in type III ELMy *H*- Mode plasma compared with the experimental data, for pedestal electron temperature and pedestal density models composed of 265 data points and 57 data points for pedestal ion temperature. It is found that the scaling law for energy confinement time IPB98(y,3) gives the best agreement with experiments, yielding RMSE of 31.08% for pedestal electron temperature and 22.90% for pedestal density, while ITERH-EPS97y scaling law for energy confinement time gives the best agreement, yielding RMSE of 23.21%.

Table 2 The RMSE% and offset values from the model based on energy distribution in type I ELMy *H*-Mode plasma.

Scaling of τ_E	**Statistic**	**Type I**		
		T_e	T_i	n_e
ITERH-93P	RMS	29.78	37.59	29.78
	Offset	-0.0020	-0.0058	0.0020
ITERH-EPS97y	RMS	27.12	70.67	27.12
	Offset	-0.0045	0.0025	0.0057
IPB98 (y,3)	RMS	28.27	72.00	28.28
	Offset	-0.0001	-0.00002	-0.0001
IPB98 (y,4)	RMS	28.00	71.05	28.00
	Offset	0.0014	-0.0040	0.0014

Table 3 The RMSE% and offset values from the model based on energy distribution in type II ELMy *H*-Mode plasma.

Scaling of τ_E	**Statistic**	**Type II**		
		T_e	T_i	n_e
ITERH-93P	RMS	15.31	11.76	15.31
	Offset	-0.0094	-0.0043	-0.0094
ITERH-EPS97y	RMS	9.02	10.96	9.02
	Offset	0.0175	0.0006	0.0175
IPB98 (y,3)	RMS	8.41	11.04	8.41
	Offset	0.0099	-0.0010	0.0099
IPB98 (y,4)	RMS	8.72	11.02	8.74
	Offset	-0.0035	-0.0068	0.0074

Table 4 The RMSE% and offset values from the model based on energy distribution in type III ELMy *H*-Mode plasma.

Scaling of τ_E	Statistic	Type III		
		T_e	T_i	n_e
ITERH-93P	*RMS*	*36.85*	*23.98*	*28.46*
	Offset	-0.0053	-0.0080	0.0037
ITERH-EPS97y	RMS	33.95	23.21	23.23
	Offset	-0.002	-0.0032	0.0020
IPB98 (y,3)	RMS	31.08	23.86	22.90
	Offset	-0.0058	-0.0016	0.0056
IPB98 (y,4)	RMS	33.29	23.93	22.99
	Offset	0.0040	0.0090	-0.0014

3.2 Uncertainty of the models

An estimate will now be made for the uncertainty in the pedestal electron, ion temperature models and pedestal density model coupled with four scaling laws for types I, II and III ELMy *H*-Mode plasmas. This estimate is motivated by the observation that the width of the distribution of any set of data points can be characterized by a standard deviation above and below the mean value. Approximately 34% of the data points lie between the mean value and what will be referred to in this paper as 'one standard deviation' above, or one standard deviation below, the mean value. For example, in the case of the pedestal electron temperature model using ITERH-93P scaling law in type I ELMy *H*-Mode plasma with $C_{E,e}$ = 0.075 in equation (8), approximately half the data points lie below the model and half the data points lie above the model (as shown in Figure 1). Hence, the model with $C_{E,e}$ = 0.075 lies at the mean value of the distribution. As the coefficient $C_{E,e}$ is varied, the fraction of data points that lie above the model changes (as shown in Figure 2). In order to estimate the range of variation needed to cover one standard deviation above and below the model for pedestal electron temperature, the coefficient $C_{E,e}$ is swept through the range of values that covers 34% of the data points above and below the standard model. That is, if $C_{E,e}$ is increased to 0.106, it is found that 34% of the data points lie between the standard model (with $C_{E,e}$ = 0.075) and this upper bound. If $C_{E,e}$ is decreased to 0.061, it is found that 34% of the data points lie between the standard model and this lower bound. In addition the upper and lower dashed lines (as shown in Figure 1) give, respectively, upper and lower bounds of predicted pedestal temperature, denoted by T_{mod}, by a linear function of experimental temperature T_{exp}. The middle solid line is the ultimate goal which gives:

$T_{mod} = T_{exp}$.

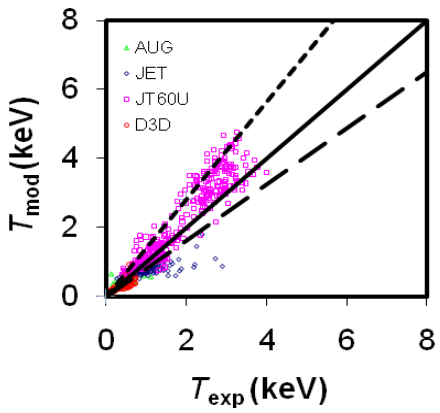

Figure 1 Using ITERH-93P scaling law in type I ELMy *H*-Mode plasma, predicted pedestal electron temperature values are plotted versus experimental pedestal electron temperature values.

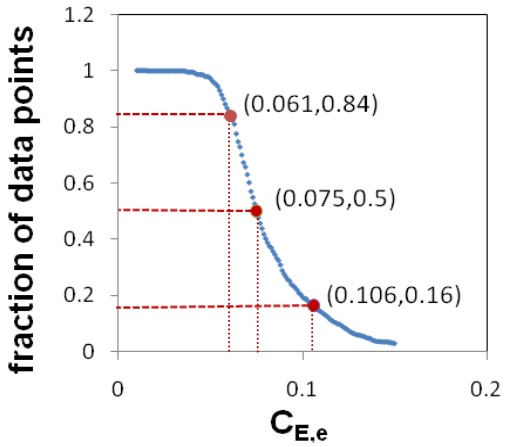

Figure 2 Fraction of experimental data point with pedestal electron temperature larger than the pedestal temperature predicted by eq. (8) as a function of the coefficient $C_{E,e}$. Points along the curve, from left to right, indicate one standard deviation below the standard model, indicate the standard model (with $C_{E,e}$ = 0.061), the standard model (with $C_{E,e}$ = 0.075), and one standard deviation above the standard model (with $C_{E,e}$ = 0.106).

Figures 1,3,4 and 5 show the comparison between the electron temperature predicted by four scaling laws and experimental data in Type I ELMy H-mode plasma. Figures 6-9 show the comparison between the ion temperature predicted by four scaling laws and experimental data in Type I ELMy H-mode plasma, and Figures 10-13 show the comparison between the density predicted by four scaling laws and experimental data in Type I ELMy H-mode plasma. In these figures, circles denote data points from DIII-D tokamak, diamonds from JET, squares from JT60U, and triangles from AUG.

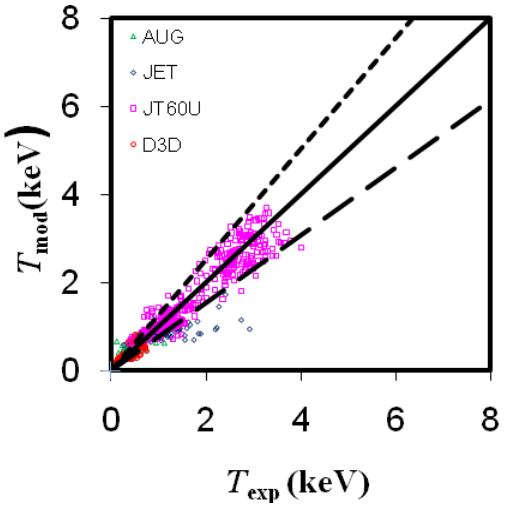

Figure 3 Using ITERH-EPS97y scaling law in type I ELMy *H*-Mode plasma, predicted pedestal electron temperature values are plotted versus experimental pedestal electron temperature values.

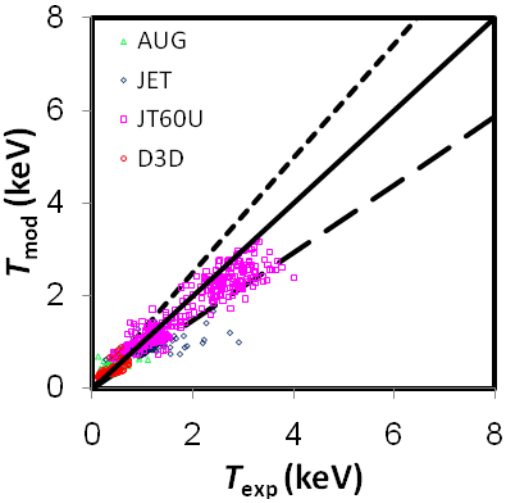

Figure 4 Using IPB98(y,3) scaling law in type I ELMy *H*-Mode plasma, predicted pedestal electron temperature values are plotted versus experimental pedestal electron temperature values

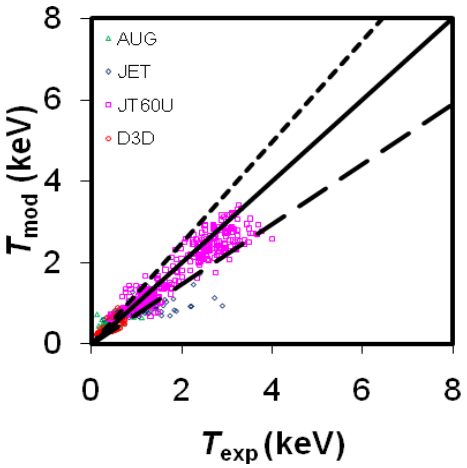

Figure 5 Using IPB98(y,4) scaling law in type I ELMy *H*-Mode plasma, predicted pedestal electron temperature values are plotted versus experimental pedestal electron temperature values**.**

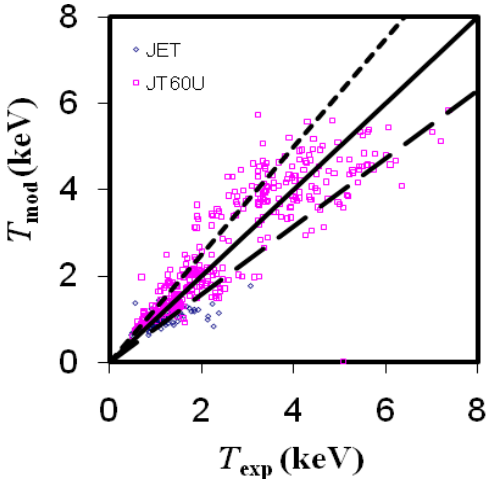

Figure 6 Using ITERH-93P scaling law in type I ELMy *H*-Mode plasma, predicted pedestal ion temperature values are plotted versus experimental pedestal ion temperature values.

In Figure 1, it is found that the predicted temperature values agree well with data from JT60U and D3D, but disagree with those from JET. For the ITERH-93P scaling law, T_{mod} can be given in terms of lower and upper bounds as $0.81T_{\exp} \le T_{\mathrm{mod}} \le 1.41T_{\exp}$. In Figure 3, it is found that the predicted temperature values agree well with data from JT60U and D3D, but disagree with those from JET. However, unlike in Figure 1, here the lower and upper bounds are closer together. For the ITERH-97y scaling law, T_{mod} can be given in terms of lower and upper bounds as $0.77T_{\exp} \le T_{\mathrm{mod}} \le 1.26T_{\exp}$. In Figures 4-5, it is found the IPB98(y,3) and IPB98(y,4) scaling laws yield qualitatively the same trends as the ITERH-EPS97y scaling law does. For the ITERH-98(y,3), T_{mod} can be given in terms of lower and upper bounds as $0.73T_{\exp} \le T_{\mathrm{mod}} \le 1.24T_{\exp}$. For the IPB98(y,4), T_{mod} can be given in terms of lower and upper bounds as $0.74T_{\exp} \le T_{\mathrm{mod}} \le 1.25T_{\exp}$.

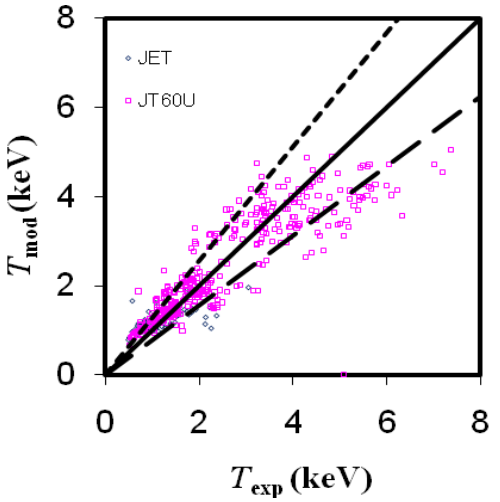

Figure 7 Using ITERH-EPS97y scaling law in type I ELMy *H*-Mode plasma, predicted pedestal ion temperature values are plotted versus experimental pedestal ion temperature values.

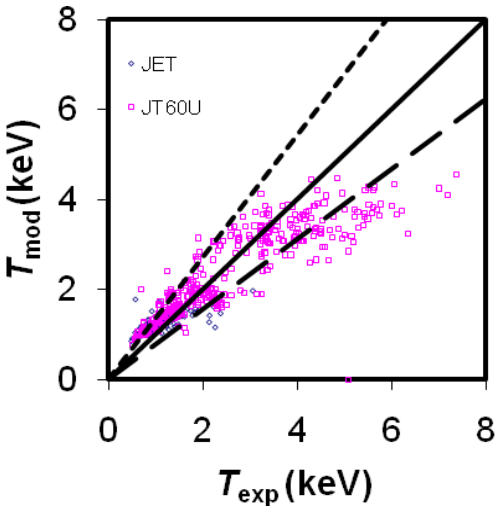

Figure 8 Using IPB98(y,3) scaling law in type I ELMy *H*-Mode plasma, predicted pedestal ion temperature values are plotted versus experimental pedestal ion temperature values.

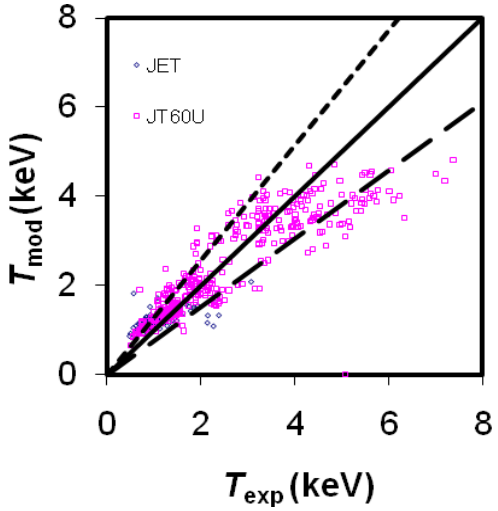

Figure 9 Using IPB98(y,4) scaling law in type I ELMy *H*-Mode plasma, predicted pedestal ion temperature values are plotted versus experimental pedestal ion temperature values.

In Figures 6-9, it is found that the predicted temperature values do not agree well with data for all scaling laws. For the ITERH-93P scaling law , T_{mod} can be given in terms of lower and upper bounds as $0.79T_{\exp} \le T_{\mathrm{mod}} \le 1.25T_{\exp}$. For the ITERH-97y scaling law, T_{mod} can be given in terms of lower and upper bounds as $0.78T_{\exp} \le T_{\mathrm{mod}} \le 1.28T_{\exp}$. For the ITERH98(y,3) scaling law, T_{mod} can be given in terms of lower and upper bounds as $0.78T_{\exp} \le T_{\mathrm{mod}} \le 1.36T_{\exp}$. For the ITERH98(y,4) scaling law, T_{mod} can be given in terms of lower and upper bounds as $0.76T_{\exp} \le T_{\mathrm{mod}} \le 1.29T_{\exp}$.

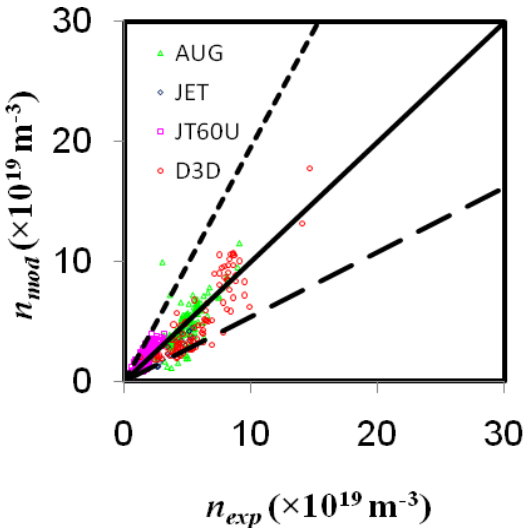

Figure 10 Using ITERH-93P scaling law in type I ELMy *H*-Mode plasma, predicted pedestal density values are plotted versus experimental pedestal density values.

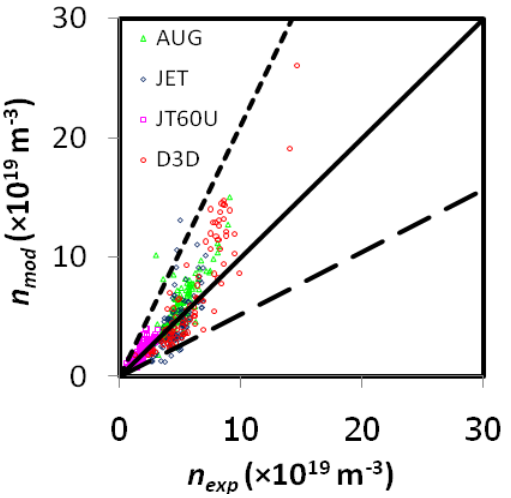

Figure 11 Using ITERH-EPS97y scaling law in type I ELMy *H*-Mode plasma,

predicted pedestal density values are plotted versus experimental pedestal density values.

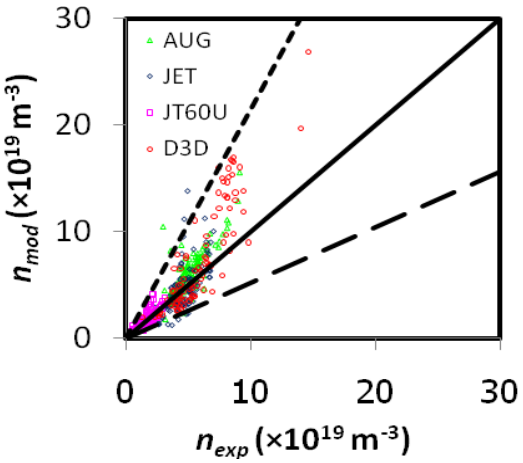

Figure12 Using IPB98(y,3) scaling law in type I ELMy *H*-Mode plasma, predicted pedestal density values are plotted versus experimental pedestal density values.

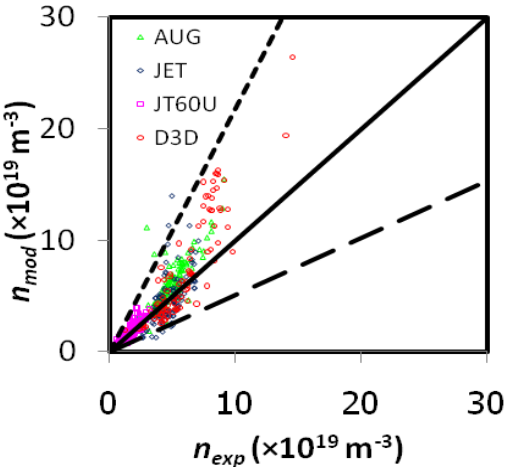

Figure 13 Using IPB98(y,4) scaling law in type I ELMy *H*-Mode plasma, predicted pedestal density values are plotted versus experimental pedestal density values.

In Figure 10, it is found that the predicted temperature values agree well with data from JT60U and JET, but disagree with those from D3D and AUG. For the ITERH-93P scaling law, T_{mod} can be given in terms of lower and upper bounds as $0.54n_{\exp} \le n_{\mathrm{mod}} \le 1.96T_{\exp}$. In Figure 11, it is found that the predicted temperature values agree well with data from JT60U, but disagree with those from D3D, JET, and AUG. For the ITERH-97y scaling law, T_{mod} can be given in terms of lower and upper bounds as $0.52n_{\exp} \le n_{\mathrm{mod}} \le 2.11T_{\exp}$. In Figure 12, it is found that the predicted temperature values agree well with data from JT60U, but disagree with those from D3D, JET, and AUG, the same as the ITERH-97y scaling law. For the ITERH98(y,3) scaling law, T_{mod} can be given in terms of lower and upper bounds as $0.52n_{\exp} \le n_{\mathrm{mod}} \le 2.15T_{\exp}$. In Figure 13, it is found that the predicted temperature values agree well with data from JT60U, but disagree with those from D3D, JET, and AUG, the same as the IPB98(y,3) scaling law. For the ITERH98 (y,4) scaling law, T_{mod} can be given in terms of lower and upper bounds as $0.51n_{\exp} \le n_{\mathrm{mod}} \le 2.19T_{\exp}$. It should be remarked from Figures 10-13 that the model based on energy distribution and on *H*-mode scaling laws tends to overpredict the pedestal density values in AUG, JET, and D3D.

The temperature of lower and upper bounds for pedestal electron and ion temperature and pedestal density in type I,II and III ELMy *H*-mode plasma are shown in Tables 5-7.

Table 5 The temperature of lower and upper bounds for pedestal electrons in types I, II and III ELMy *H*-mode plasmas.

Scaling of τ_E	Type I		Type II		Type III	
	lower	upper	lower	upper	lower	upper
ITERH-93P	0.81	1.41	0.92	1.12	0.76	1.86
ITERH-EPS97y	0.77	1.26	0.93	1.09	0.77	1.66
IPB98 (y,3)	0.73	1.24	0.92	1.08	0.77	1.49
IPB98 (y,4)	0.74	1.25	0.93	1.09	0.76	1.60

Table 6 The temperature of lower and upper bounds for pedestal ions in type I, II, and III ELMy *H*-mode plasmas.

Scaling of τ_E	Type I		Type II		Type III	
	lower	upper	lower	upper	lower	upper
ITERH-93P	0.79	1.25	0.89	1.10	0.79	1.25
ITERH-EPS97y	0.78	1.28	0.89	1.08	0.82	1.47
IPB98 (y,3)	0.78	1.36	0.89	1.07	0.79	1.26
IPB98 (y,4)	0.76	1.29	0.89	1.11	0.83	1.26

Table 7 The pedestal density of lower and upper bounds in types I, II, and III ELMy *H*-mode plasma.

Scaling of τ_E	Type I		Type II		Type III	
	lower	upper	lower	upper	lower	upper
ITERH-93P	0.54	1.25	0.92	1.10	0.77	1.25
ITERH-EPS97y	0.52	1.28	0.93	1.08	0.78	1.47
IPB98 (y,3)	0.52	1.36	0.92	1.07	0.77	1.26
IPB98 (y,4)	0.51	1.29	0.93	1.11	0.76	1.26

4. Conclusion

For pedestal electron temperature in a type I ELMy *H*-mode plasma, it is found that the ITERH-EPS97y scaling law gives the best agreement with the experimental data, yielding RMSE of 27.12%, while the IPB98(y,3) scaling law gives the best agreement with the experimental data for types II and III, yielding RMSE of 8.41% and 31.08%, respectively. For the pedestal ion temperature in type I ELMy *H*-mode plasma, it is found that the ITERH-93P scaling law gives the best agreement with the experimental data, yielding RMSE of 37.59%, while the ITERH-EPS97y scaling law gives the best agreement with the experimental data for types II and III, yielding RMSE of 10.96% and 23.21%, respectively. And for pedestal density in a type I ELMy *H*-mode plasma, it is found that the ITERH-EPS97y scaling law gives the best agreement with the experimental datas, yielding RMSE of 27.12%, while the IPB98(y,3) scaling law gives the best agreement with the experimental data, for types II and III, yielding RMSE of 8.41% and 22.90%, respectively, the same as pedestal electron temperature.

5. Acknowledgments

This work is supported by the Commission on Higher Education (CHE) and the Thailand Research Fund (TRF) under Contract No.RMU5180017, and the Thailand National Research University Project. W. Buangam thanks the Development and Promotion of Science and

Technology talents project (DPST) for providing a grant fund for this research.

6. References

[1] H. Zohm, Plasma. Phys. Control. Fusion, Vol. 38, pp. 105-128, 1996.

[2] G. Bateman *et al*, Phys. Plasmas, Vol. 5, p. 1793, 1998.

[3] D. Hannum *et al*, Phys. Plasmas, Vol. 8, p. 964, 2001.

[4] J. G. Cordey, Nucl. Fusion, Vol. 43, pp. 670–674, 2003.

[5] J.E. Kinsey, Nucl. Fusion, Vol. 43, pp.1845–1854, 2003.

[6] T. Onjun, Ph. D. Thesis, Lehigh University, 2004.

[7] J. Rapp et al, Proceedings of the 22nd IAEA Fusion Energy Conference, Geneva, Switzerland (13th-18th October 2008)

[8] T. Onjun *et al*, Phys. Plasmas, Vol. 9, p. 5018, 2002.

[9] J. G. Cordey et al, Nucl. Fusion, Vol. 39, pp. 301–307, 1999.

[10] D. McDonald et al, Nucl. Fusion, Vol. 47, p.147, 2007.

[11] ITER Physics Basis, Nucl. Fusion, Vol. 47, S18, 2007.

[12] R. J. Goldston, Plasma Phys. Control. Fusion, Vol. 26 No. 1A,87, 1984.

[13] N. A. Uckan, Workshop on Physics Issues for FIRE, May 1–3, 2000, Princeton, NJ.

[14] T. Onjun *et al*, Phys. Plasmas, Vol. 8, p. 975,2001.

[15] J. Freidberg, Plasma Physics and Fusion Energy, Cambridge Univ. Press, Cambridge, 2007.

[16] W. M. Stacey, Fusion Plasma Physics,Weinheim; Chichester: Wiley-VCH; John Wiley, distributor 2005.

[17] J. Wesson, Tokamaks, 3rd Edition, Clarendon Press, Oxford, 2004.

[18] D. Boucher et al, Nucl. Fusion, Vol. 40, p. 1955, 2000.